Non-double-couple mechanisms in weak transverse isotropy

Václav Vavryčuk

Geophysical Institute, Academy of Sciences of the Czech Republic, Boční II, 141 31 Praha 4, Czech Republic, E-mail: vv@ig.cas.cz

Abstract

Shear faulting in anisotropic rocks produces non-double-couple (non-DC) mechanisms. The non-DC components can combine the isotropic (ISO) and compensated linear vector dipole (CLVD) components. The formulas for percentages of the ISO and CLVD are simplified under the assumption of weak transverse isotropy and they can be advantageously expressed in terms of the Thomsen's weak anisotropy parameters. Shear faulting in crustal rocks with anisotropy strength of 10 % can produce the ISO up to 10% and the CLVD up to 30%. Such values are significant and detectable in carefully determined focal mechanisms.

1. INTRODUCTION

Focal mechanisms of earthquakes bring valuable information on the orientation of fractures, on type of faulting, pore pressure or tectonic stress in a seismically active area. In exploration geophysics, the focal mechanisms are often determined for micro-earthquakes induced in reservoirs during the gas or oil production or during the well stimulation by hydraulic fracturing (Rutledge & Phillips 2003). The knowledge of focal mechanisms helps in enhancing the reservoir characterization by imaging the orientation, complexity and temporal growth of induced fractures and by mapping of faults (Maxwell & Urbancic 2001). Focal mechanisms can also be utilized in estimating pore pressure. If pore pressure is low, we observe shear faulting characterized by double-couple mechanisms; if pore pressure is high, we can observe tensile faulting and the focal mechanisms are non-double-couple (Vavryčuk 2001, 2002).

So far focal mechanisms have been determined and interpreted under the assumption of isotropic medium. However, the geological structures of the Earth crust frequently display anisotropy (Thomsen 1986; Babuška & Cara 1991; Tsvankin 2001), which can be caused by sediment layering, presence of aligned microcracks, cracks or fractures, or by the textural ordering of rock-forming minerals. Anisotropy significantly affects propagation of seismic waves (Musgrave 1970; Helbig 1994; Coates & Chapman 1990; Kravtsov & Orlov 1990; Bulant & Klimeš 2004; Klimeš & Bulant 2004) but also it affects properties of seismic sources that become more complicated (Kawasaki & Tanimoto 1981; Julian *et al.* 1998; Roessler *et al.* 2004; Vavryčuk 2004). For example, Vavryčuk (2005) has shown that double-couple mechanisms produced by shear faulting under isotropy become non-double-couple under anisotropy. Also the fault plane solutions calculated under the assumption of isotropy can deviate from the true orientations provided the source area is actually anisotropic (Šílený & Vavryčuk 2002).

In this paper, I continue in work done by Vavryčuk (2005) where focal mechanisms in general anisotropy of arbitrary symmetry and of arbitrary strength are studied. I specify this theory for weak transverse isotropy that is the most common type of anisotropy used in exploration geophysics. I apply the first-order perturbation theory (Pšenčík & Gajewski 1998; Vavryčuk & Pšenčík 1998; Pšenčík & Dellinger 2001; Farra 2004, 2005) and derive approximate formulas for the non-double couple components produced by shear faulting in transversely isotropic media. The formulas are expressed using the Thomsen's weak anisotropy parameters (Thomsen 1986; Tsvankin & Thomsen 1994). The accuracy of the derived approximations are tested on theoretical models of crustal anisotropy as well as on anisotropy observed on crustal rock samples.

2. MOMENT TENSORS IN ANISOTROPIC MEDIA

The moment tensor **M** of a seismic source situated in an anisotropic medium is expressed as (Vavryčuk 2005, Eq. 4)

$$M_{ij} = c_{ijkl} D_{kl} \ . \tag{1}$$

Tensor c_{ijkl} is the tensor of elastic parameters of the anisotropic medium surrounding the fault, and tensor **D** denotes the seismic source tensor

$$D_{kl} = \frac{uS}{2}(\nu_k n_l + \nu_l n_k) \tag{2}$$

where u is the slip, S is the fault area, $\boldsymbol{\nu}$ is the slip direction, and **n** is the fault normal. If vectors $\boldsymbol{\nu}$ and **n** are perpendicular ($\boldsymbol{\nu} \perp \mathbf{n}$), we speak of shear faulting; if they are arbitrarily oriented, we speak of tensile faulting.

In general, the moment tensors in anisotropic media are complicated. They consist of the double couple (DC), linear vector dipole (CLVD) and isotropic (ISO) parts

$$\mathbf{M} = \mathbf{M}^{ISO} + \mathbf{M}^{CLVD} + \mathbf{M}^{DC}, \tag{3}$$

which are defined as follows (Jost & Hermann 1989; Vavryčuk 2005)

$$\mathbf{M}^{ISO} = \frac{1}{3}\mathrm{Trace}(\mathbf{M}) \begin{bmatrix} 1 & 0 & 0 \\ 0 & 1 & 0 \\ 0 & 0 & 1 \end{bmatrix}, \tag{4}$$

$$\mathbf{M}^{CLVD} = \left|\varepsilon^{CLVD}\right| M^{*}_{|MAX|} \begin{bmatrix} -1 & 0 & 0 \\ 0 & -1 & 0 \\ 0 & 0 & 2 \end{bmatrix}, \tag{5}$$

$$\mathbf{M}^{DC} = \left(1 - 2\left|\varepsilon^{CLVD}\right|\right) M^{*}_{|MAX|} \begin{bmatrix} -1 & 0 & 0 \\ 0 & 0 & 0 \\ 0 & 0 & 1 \end{bmatrix}. \tag{6}$$

Parameter ε^{CLVD} measures the size of CLVD relative to DC and is defined as:

$$\varepsilon^{CLVD} = -\frac{M^*_{|MIN|}}{\left|M^*_{|MAX|}\right|}, \tag{7}$$

where $M^*_{|MAX|}$ and $M^*_{|MIN|}$ are the eigenvalues of deviatoric moment $\mathbf{M}^* = \mathbf{M}^{CLVD} + \mathbf{M}^{DC}$ with the maximum and minimum absolute values, respectively. To assess relative amounts of the DC, CLVD and ISO components in a moment tensor, we usually calculate their percentages:

$$ISO = \frac{1}{3}\frac{\mathrm{Trace}(\mathbf{M})}{\left|M_{|MAX|}\right|}\cdot 100\%, \tag{8}$$

$$CLVD = 2\varepsilon^{CLVD}\left(100\% - |ISO|\right), \tag{9}$$

$$DC = 100\% - |ISO| - |CLVD|, \tag{10}$$

where $M_{|MAX|}$ denotes that eigenvalue of **M,** which has the maximum absolute value.

3. MOMENT TENSORS IN ISOTROPIC MEDIA

The moment tensors considerably simplify under the assumption of isotropy. Taking into account that the elastic parameters c_{ijkl} can be expressed by the Lamé constants as

$$c_{ijkl} = \lambda\delta_{ij}\delta_{kl} + \mu\left(\delta_{ik}\delta_{jl} + \delta_{il}\delta_{jk}\right), \tag{11}$$

Eq. (1) yields

$$M_{ij} = \lambda D_{kk}\delta_{ij} + 2\mu D_{ij}. \tag{12}$$

Diagonalizing this moment tensor, we obtain (Vavryčuk 2005, eq. 42)

$$\mathbf{M}^{diag} = uS\begin{bmatrix} (\lambda+\mu)\mathbf{n}\cdot\mathbf{v}+\mu & 0 & 0 \\ 0 & \lambda\mathbf{n}\cdot\mathbf{v} & 0 \\ & & (\lambda+\mu)\mathbf{n}\cdot\mathbf{v}-\mu \end{bmatrix}. \tag{13}$$

This moment tensor is referred to the coordinate system of eigenvectors of $\mathbf{M}$

$$\mathbf{e}_1 = \frac{\mathbf{n}+\mathbf{v}}{|\mathbf{n}+\mathbf{v}|}\ ,\ \mathbf{e}_2 = \mathbf{n}\otimes\mathbf{v},\ \mathbf{e}_3 = \frac{\mathbf{n}-\mathbf{v}}{|\mathbf{n}-\mathbf{v}|}, \tag{14}$$

where symbol $\otimes$ denotes the vector product. If we assume that the source is shear, then

$$\mathbf{n}\cdot\mathbf{v} = n_1v_1 + n_2v_2 + n_3v_3 = 0\ , \tag{15}$$

and Eq. (13) further simplifies to

$$\mathbf{M}^{diag} = \mu uS\begin{bmatrix} +1 & 0 & 0 \\ 0 & 0 & 0 \\ 0 & 0 & -1 \end{bmatrix}, \tag{16}$$

which represents the pure double-couple source. Hence, shear faulting in isotropic media generates no CLVD and ISO components.

4. SHEAR FAULTING IN WEAK TRANSVERSE ISOTROPY

4.1. Thomsen's weak anisotropy parameters

Let us assume a shear source situated in a weakly transversely isotropic (TI) medium. The medium will be described by the elastic parameters of the isotropic background c_{33} and c_{44}, and by Thomsen's weak anisotropy parameters (Thomsen 1986; Tsvankin & Thomsen 1994):

$$\varepsilon = \frac{c_{11} - c_{33}}{2c_{33}}, \tag{17}$$

$$\gamma = \frac{c_{66} - c_{44}}{2c_{44}} \tag{18}$$

$$\sigma = \frac{1}{2c_{44}}\left(c_{11} - c_{44} - \frac{(c_{13} + c_{44})^2}{c_{33} - c_{44}} \right) \tag{19}$$

where c_{kl} are the elastic parameters in the Voigt notation. The elastic parameters are referred to the coordinate system in which the symmetry axis is along the vertical. The Thomsen's parameters ε, γ and σ can serve as a measure of strength of TI: they are zero for isotropy and close to zero for weak anisotropy. Geometry of faulting will be fixed with fault normal $\mathbf{n} = (0,0,1)^T$ and slip direction $\mathbf{v} = (1,0,0)^T$. The symmetry axis of TI will be inclined being specified by spherical angles θ and φ, $\mathbf{m} = (\sin\varphi\sin\theta, \cos\varphi\sin\theta, \cos\theta)^T$.

4.2. Moment tensors

Since anisotropy is weak, we can express the moment tensor as the sum of the moment tensor produced by shear faulting in the isotropic background $\mathbf{M}^0$ and of its perturbation $\Delta\mathbf{M}$ produced by anisotropy

$$\mathbf{M} = \mathbf{M}^0 + \Delta\mathbf{M}, \tag{20}$$

where

$$\mathbf{M}^0 = \begin{bmatrix} 0 & 0 & M_0 \\ 0 & 0 & 0 \\ M_0 & 0 & 0 \end{bmatrix}, \; \Delta\mathbf{M} = \begin{bmatrix} \Delta M_{11} & \Delta M_{12} & \Delta M_{13} \\ \Delta M_{12} & \Delta M_{22} & \Delta M_{23} \\ \Delta M_{13} & \Delta M_{23} & \Delta M_{33} \end{bmatrix} \text{ and } M_0 = uSc_{44}. \tag{21}$$

The components of $\Delta\mathbf{M}$ are expressed in terms of Thomsen's weak anisotropy parameters as follows:

$$\begin{aligned}
\Delta M_{11} &= M_0 m_1 m_3 \left[-\kappa\varepsilon + \sigma\left(2m_1^2 - 1\right)\right] \\
\Delta M_{22} &= M_0 m_1 m_3 \left[-\kappa\varepsilon + \sigma\left(2m_2^2 - 1\right) + 4\gamma\right] \\
\Delta M_{33} &= M_0 m_1 m_3 \left[-\kappa\varepsilon + \sigma\left(2m_3^2 - 1\right)\right] \\
\Delta M_{12} &= 2M_0 m_2 m_3 \left(-\gamma + \sigma m_1^2 \right) \\
\Delta M_{13} &= 2M_0 \left(\gamma m_2^2 + \sigma m_1^2 m_3^2 \right) \\
\Delta M_{23} &= 2M_0 m_1 m_2 \left(-\gamma + \sigma m_3^2 \right)
\end{aligned} \tag{22}$$

where

$$\kappa = c_{33} / c_{44} \; . \tag{23}$$

The trace of the moment tensor reads

.

$$\mathrm{Tr}(\mathbf{M}) = \mathrm{Tr}(\Delta\mathbf{M}) = M_0 m_1 m_3 \left(-3\kappa\varepsilon + 4\gamma - \sigma \right), \tag{24}$$

hence it is zero for isotropic media but generally non-zero for weak TI. Using formulas for calculating the perturbation of eigenvalues of tensor **M** (Korn & Korn 2000)

$$\Delta M_1 = \Delta M_{kl} e_{1k} e_{1l} \ , \ \Delta M_2 = \Delta M_{kl} e_{2k} e_{2l} \ , \ \Delta M_3 = \Delta M_{kl} e_{3k} e_{3l} \ , \tag{25}$$

we obtain

$$\Delta M_1 = M_0 m_1 m_3 (-\kappa\varepsilon + 2\sigma m_1 m_3) + M_0 m_2^2 (2\gamma - \sigma m_1 m_3) \ ,$$

$$\Delta M_2 = M_0 m_1 m_3 \left[-\kappa\varepsilon + \sigma(2m_2^2 - 1) + 4\gamma\right] \ , \tag{26}$$

$$\Delta M_3 = M_0 m_1 m_3 (-\kappa\varepsilon - 2\sigma m_1 m_3) - M_0 m_2^2 (2\gamma + \sigma m_1 m_3) \ ,$$

where vectors $\mathbf{e}_1$, $\mathbf{e}_2$ and $\mathbf{e}_3$ are the eigenvectors of the moment tensor $\mathbf{M}^0$ referred to the isotropic background,

$$\mathbf{e}_1 = \frac{1}{\sqrt{2}}(1,0,1)^T \ , \ \mathbf{e}_2 = (0,1,0)^T \ , \ \mathbf{e}_3 = \frac{1}{\sqrt{2}}(-1,0,1)^T \tag{27}$$

4.3. Non-DC components

Assuming that perturbations ΔM_1, ΔM_2 and ΔM_3 are small with respect to M_0 and applying the first-order perturbation theory, we can derive approximate formulas for percentages of ISO and CLVD components in the moment tensors. Since

$$M^*_{|MIN|} = \Delta M_2 - \frac{1}{3}\mathrm{Tr}(\mathbf{M}) = -\frac{1}{3}(\Delta M_1 + \Delta M_3 - 2\Delta M_2) \ , \tag{29}$$

$$\left|M_{|MAX|}\right| = \max\left(M_0 + \Delta M_1, M_0 - \Delta M_3\right) \ , \tag{30}$$

$$\left|M^*_{|MAX|}\right| = \max\left(M_0 - \frac{1}{3}\left(\Delta M_2 + \Delta M_3 - 2\Delta M_1\right), M_0 + \frac{1}{3}\left(\Delta M_1 + \Delta M_2 - 2\Delta M_3\right)\right) \ , \tag{31}$$

we get from Eqs (7) and (8)

$$ISO \cong 100\% \cdot \frac{\Delta M_1 + \Delta M_2 + \Delta M_3}{3M_0} \ , \tag{32}$$

$$\varepsilon^{CLVD} \cong \frac{\Delta M_1 + \Delta M_3 - 2\Delta M_2}{3M_0} \ . \tag{33}$$

Substituting equations (26) into (32)-(33) we finally obtain

$$ISO \cong 100\% \cdot \frac{1}{3} m_1 m_3 \left(-3\kappa\varepsilon + 4\gamma - \sigma\right) \ , \tag{34}$$

$$\varepsilon^{CLVD} \cong \frac{2}{3} m_1 m_3 \left[-4\gamma + \sigma\left(1 - 3m_2^2\right)\right] . \tag{35}$$

The CLVD can be obtained by inserting (34) and (35) into (9).

More accurate equations than (34) and (35) can be derived, if $\left|M_{|MAX|}\right|$ and $\left|M^*_{|MAX|}\right|$ are calculated correctly by (29) and (30) but not substituted simply by M_0. This approach yields

$$ISO \cong 100\% \cdot \frac{1}{3C_1} m_1 m_3 \left(-3\kappa\varepsilon + 4\gamma - \sigma\right) \ , \tag{36}$$

$$\varepsilon^{CLVD} \cong \frac{2}{3C_2} m_1 m_3 \left[-4\gamma + \sigma\left(1 - 3m_2^2\right)\right] , \tag{37}$$

where

$$C_1 = \max\left(1 + m_1 m_3 (\mp \kappa\varepsilon + 2\sigma m_1 m_3) + m_2^2 (2\gamma \mp \sigma m_1 m_3)\right),$$

$$C_2 = \max\left(1 + \frac{2}{3}\gamma(3m_2^2 \mp 2m_1 m_3) + \frac{1}{3}\sigma m_1 m_3 (6m_1 m_3 \mp 3m_2^2 \pm 1)\right),$$

and we used the following notation

$$\max(a \pm b \mp c) = \max(a + b - c, a - b + c).$$

5. APPLICATION TO CRUSTAL ROCKS

In this section, the derived formulas are applied to theoretical models of crustal anisotropy and to anisotropy observed on crustal rock samples. I consider four theoretical anisotropy models: one model produced by presence of aligned water-filled cracks and three models produced by layering. The effective anisotropy is calculated by the Hudson (1981) theory for cracks, and by the Backus (1962) averaging for layers. Furthermore, I consider 10 published models of anisotropy observed on rocks. The anisotropy was measured in the laboratory on rock samples, which originate from the upper crust and represent mainly anisotropic sedimentary and metamorphic rocks. Of course, the presented models do not cover all possible variations of anisotropy at focal areas, but still they can give an insight of how significant non-DC components can be generated by shear faulting in the crust and how accurate are the presented approximations for the calculation of the non-DC components.

The anisotropy models are summarized in Tab. 1. The table presents the Thomsen's weak anisotropy parameters of each model together with the identification of the rock sample or of the model, and the reference. Since some of the models were defined by standard elastic parameters (Shearer & Chapman 1989; Baptie *et al.* 1995; Rabbel *et al.* 2004; Goldfrey *et al.* 2000), the weak anisotropy parameters presented in the table had to be calculated using

formulas (17)-(19). Table 2 summarizes anisotropy strength of *P*, *SV* and *SH* waves and maximum absolute values of the CLVD and ISO components generated by shear faulting in the specified anisotropy model. Anisotropy strength is defined as

$$a = 200\% \cdot \frac{v^{\mathrm{MAX}} - v^{\mathrm{MIN}}}{v^{\mathrm{MAX}} + v^{\mathrm{MIN}}}, \tag{38}$$

where v^{MAX} and v^{MIN} are the maximum and minimum phase velocities of the respective wave. When calculating the maximum values of the CLVD and ISO, the geometry of faulting was fixed and the direction of the symmetry axis varied in a grid of spherical angles θ and φ with step of 2°. The CLVD and ISO were calculated using exact formulas (8)-(9) and approximate formulas (34)-(35) and (36)-(37).

The directional variation of the phase velocities is exemplified for the Layers II model (see Tab. 1) in Figs. 1 and 2. The anisotropy strength is 13.1, 8.1 and 12.4% for the *P*, *SV* and *SH* waves (se Tab. 2). Shear faulting in this anisotropy generates the maximum ISO and CLVD components of 14.4% and 18.7%. The directional variation of the exact values of the ISO and CLVD together with errors produced by approximate formulas (34)-(35) and (36)-(37) are shown in Figs 3 and 4. The errors are almost 6 and 4% for the ISO and CLVD components in the case of formulas (34)-(35). Formulas (36)-(37) yield more accurate results yielding the maximum errors in the ISO and CLVD of 0.04 and 0.8%.

Fig. 3a shows that the exact ISO component for Layers II has one maximum and one minimum which lie in the plane of the slip and fault normal. The same or a very similar pattern can be observed also for the other anisotropy models (see Fig. 5). However, the directional variation of the CLVD component is more variable for various anisotropy models, and it can also be more complicated. As regards the Layers II model, the CLVD displays two maxima and two minima which lie off the plane defined by the slip and fault normal (see Fig 4a), but other models can produce less or higher number of local maxima and minima (see Fig. 6).

Table 1. Anisotropy models

Model/rock	v^P [km/s]	v^S [km/s]	ε	γ	δ	ρ [g/cm^3]	Model/rock identification	Reference
Theoretical models								
Cracks	4.477	2.258	0.005	0.125	-0.111	2.80	Model 1	Shearer & Chapman (1989)
Layers I	3.907	2.185	0.021	0.015	0.008	2.60	PTL1	Baptie *et al.* (1995, table 1)
Layers II	3.091	1.749	0.150	0.141	0.023	2.60	PTL2	Baptie *et al.* (1995, table 1)
Layers III	2.585	1.472	0.323	0.318	0.032	2.60	PTL3	Baptie *et al.* (1995, table 1)
Rocks								
Sandstone I	4.476	2.814	0.097	0.051	0.091	2.50	Mesaverde (4912) immature sandstone	Thomsen (1986, table 1)
Sandstone II	4.099	2.346	0.077	0.066	0.010	2.45	Mesaverde (4946) immature sandstone	Thomsen (1986, table 1)
Sandstone III	4.349	2.571	0.091	0.105	0.148	2.46	Mesaverde (5481.3) immature sandstone	Thomsen (1986, table 1)
Shale I	3.901	2.682	0.137	0.026	-0.012	2.64	Mesaverde shale (1599)	Thomsen (1986, table 1)
Shale II	4.721	2.890	0.135	0.180	0.205	2.64	Cotton Valley shale	Thomsen (1986, table 1)
Shale III	2.202	0.969	0.015	0.030	0.060	2.25	Pierre shale (z = 950 m)	Thomsen (1986, table 1)
Gneiss I	6.000	3.380	0.043	0.125	-0.007	2.78	KTB (2.2-3.0 km)	Rabbel *et al.* (2004, table 1)
Gneiss II	5.109	3.126	0.215	0.222	0.107	2.75	KTB (7.9-8.2 km)	Rabbel *et al.* (2004, table 1)
Phyllite	5.947	3.438	0.100	0.149	-0.043	2.72	Chugach phyllite, TA-2, p = 100 MPa	Godfrey *et al.* (2000, table 1)
Schist	5.727	3.439	0.150	0.049	0.085	2.72	Pelona schist, LA-1, p = 100 MPa	Godfrey *et al.* (2000, table 1)

v^P and v^S are vertical P and S velocities, ε, γ and δ are weak anisotropy parameters, and ρ is the density.

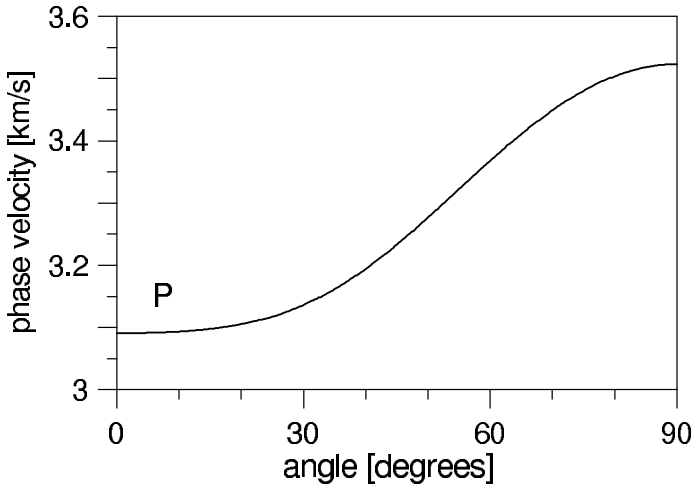

Figure 1. Phase velocity of the *P* wave as a function of the angle between the wave normal and the symmetry axis for the Layers II model.

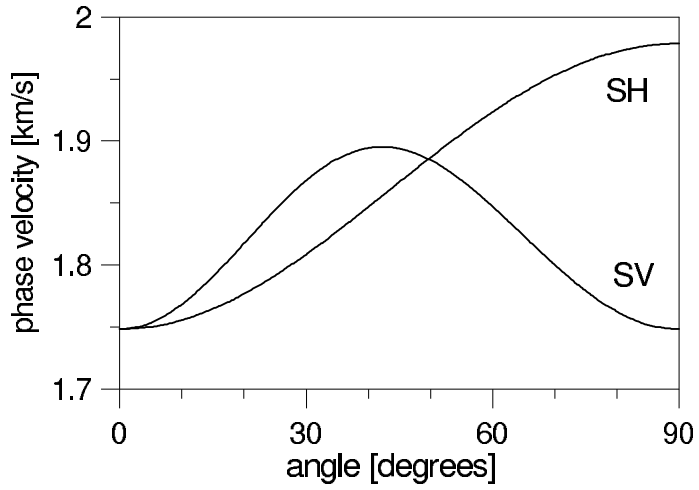

Figure 2. Phase velocity of the *SV* and *SH* waves as a function of the angle between the wave normal and the symmetry axis for the Layers II model.

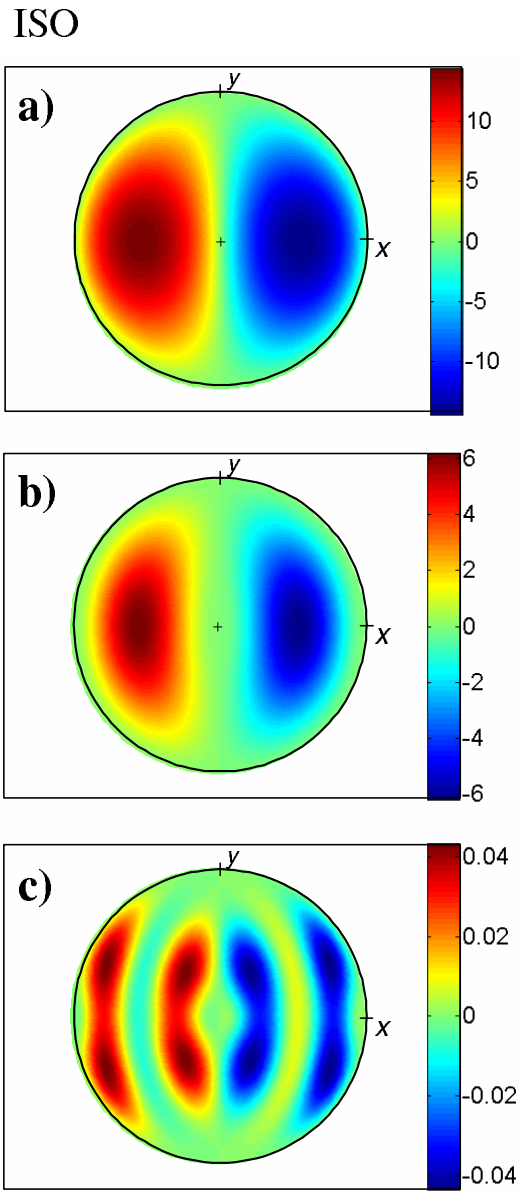

Figure 3. The percentage of the exact (a) and approximate (b-c) ISO components generated by shear faulting in the Layers II model with an inclined symmetry axis. Geometry of faulting is fixed: $\mathbf{n} = (0,0,1)^T$, and $\mathbf{v} = (1,0,0)^T$. Points inside the circle correspond to transverse isotropy (TI) with a varied orientation of the symmetry axis. The plus sign marks the TI with the vertical symmetry axis, the points along the circle correspond to the TI with horizontal symmetry axes. The color indicates: (a) the exact value of the ISO; (b) the approximate value of the ISO calculated by eqs (34)-(35), and (c) the approximate value of the ISO calculated by eqs (36)-(37). Equal-area projection is used.

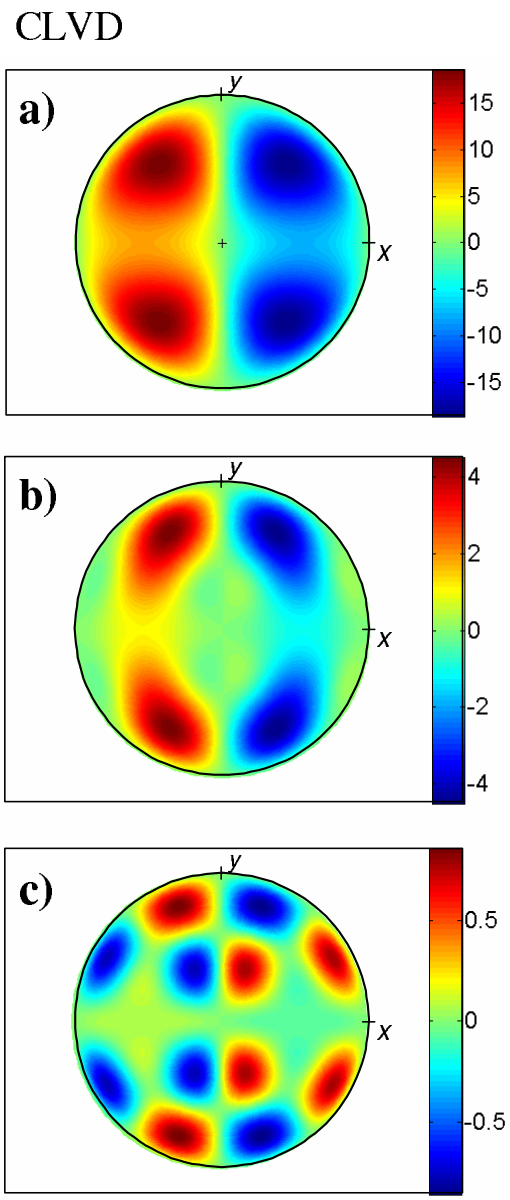

Figure 4. The percentage of the exact (a) and approximate (b-c) CLVD components generated by shear faulting in the Layers II model with an inclined symmetry axis. Equal-area projection is used. The plus sign marks the vertical symmetry axis. For details, see the caption of Fig. 3.

Table 2. Anisotropy strength and percentages of ISO and CLVD,

Model/rock	a^P [%]	a^{SV} [%]	a^{SH} [%]	ISO^{MAX} [%]	ISO_1^{MAX} [%]	ISO_2^{MAX} [%]	$CLVD^{MAX}$ [%]	$CLVD_1^{MAX}$ [%]	$CLVD_2^{MAX}$ [%]
Theoretical models									
Cracks	3.5	11.0	11.2	0.6	0.1	0.1	19.9	24.3	19.6
Layers I	2.1	1.0	1.5	2.9	3.1	2.9	2.6	2.6	2.6
Layers II	13.1	8.1	12.4	14.4	20.6	14.4	18.7	22.8	18.8
Layers III	24.8	15.2	24.5	22.4	43.5	22.4	31.7	44.9	32.2
Rocks									
Sandstone I	8.9	0.3	4.9	8.2	9.1	8.1	10.2	11.4	11.2
Sandstone II	7.2	4.6	6.2	8.8	10.8	8.8	10.4	11.6	10.4
Sandstone III	8.4	3.6	9.5	3.7	3.3	3.1	33.9	37.6	37.0
Shale I	12.1	6.6	2.5	13.8	18.0	13.8	10.2	11.5	10.2
Shale II	11.9	3.9	15.3	3.6	2.9	2.7	49.8	58.7	55.6
Shale III	1.9	5.9	2.9	2.0	2.0	2.2	23.6	23.0	24.4
Gneiss I	4.1	3.6	11.2	0.8	0.9	0.8	20.3	23.4	20.4
Gneiss II	17.9	5.5	18.3	13.3	18.8	13.1	27.5	35.1	28.8
Phyllite	9.5	9.3	13.0	9.0	12.2	8.9	20.4	25.5	20.5
Schist	13.1	3.7	4.7	15.9	20.6	15.9	8.2	8.6	8.0

Quantities a^P, a^{SV} *and* a^{SH} denote anisotropy strength of *P*, *SV* and *SH* waves, which is defined on (38). ISO^{MAX} and $CLVD^{MAX}$ are the exact maximum absolute values of the isotropic (ISO) and compensated linear vector dipole (CLVD) components. ISO_1^{MAX} and $CLVD_1^{MAX}$ are the approximate values calculated by eqs (34)-(35), and ISO_2^{MAX} and $CLVD_2^{MAX}$ are approximate values calculated by eqs (36)-(37).

The anisotropy models presented in Tabs 1 and 2 cover the interval of anisotropy strength from 2 to almost 25%. Shear faulting in the models produces the maximum ISO component in the range from 0.6 to 22.4% and the maximum CLVD from 2.6 to 49.8%. Usually, the CLVD component is higher than the ISO component but for some models (Shale I, Schist) the other case is also observed. Interestingly, some models with a rather weak

anisotropy generate a considerably high CLVD. This applies, for example, to Shale III of anisotropy strength less than 6% which generates the CLVD of 23.6%, or to Sandstone III of anisotropy strength less than 10% but with the CLVD of 33.9%. This implies that shear faulting in crustal rocks can really generate detectable and significant non-DC components owing to anisotropy.

6. CONCLUSIONS

Shear faulting in anisotropic rocks produces non-double couple mechanisms. The non-DC mechanisms can be exploited for determining geometry of faulting and anisotropy in the source area (Vavryčuk 2004). Under weak anisotropy, the formulas for the percentages of the non-DC components CLVD and ISO can be simplified using the first-order perturbation theory. Under weak transverse isotropy, the CLVD and ISO can be expressed using the Thomsen's weak anisotropy parameters. If we fix the fault normal and slip direction and vary the orientation of the symmetry axis, the ISO component has an identical directional variation for all values of weak anisotropy parameters. The maxima and minima of the ISO produced by shear faulting in weak transverse isotropy are generated if the symmetry axis lies in the plane of the fault normal and slip and is inclined by 45° from the fault normal. The directional variation of the CLVD is more variable and can be more complicated. The maxima and minima can lie off the plane of the fault normal and slip. Usually, the CLVD is more pronounced than ISO and it can attain values higher than 30% for anisotropy with strength of 10% or less. Hence, anisotropy of rocks can significantly affect focal mechanisms and thus it should be taken into account in their interpretations.

Acknowledgements

The work was supported by the Grant Agency of the Academy of Sciences of the Czech Republic, Grant No. A3012309, by the Consortium Project SW3D "Seismic waves in complex 3-D structures", and by the EU consortium project IMAGES "Induced microseismics applications from global earthquake studies", contract No. MTKI-CT-2004-517242.

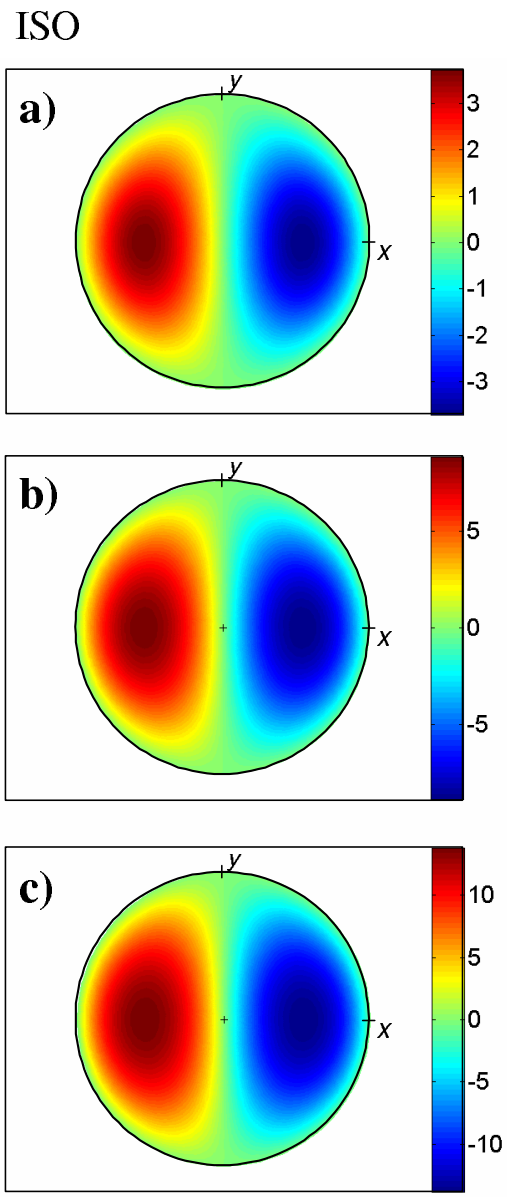

Figure 5. The percentage of the exact ISO components generated by shear faulting in the: (a) Sandstone III model, (b) Sandstone II model, and (c) Shale I model. For details, see the caption of Fig. 3.

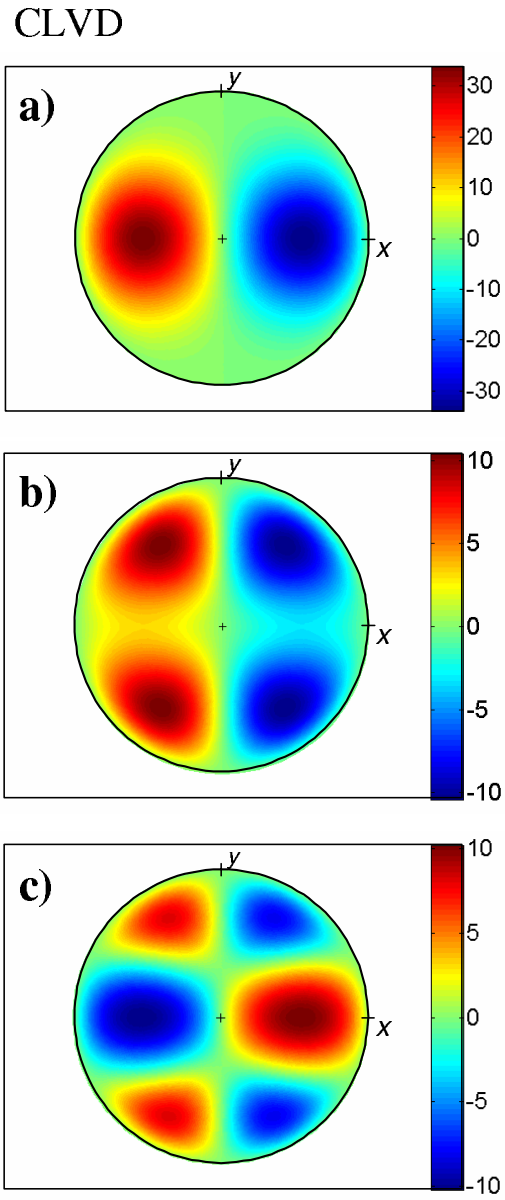

Figure 6. The percentage of the exact CLVD components generated by shear faulting in the: (a) Sandstone III model, (b) Sandstone II model, and (c) Shale I model. For details, see the caption of Fig. 3.

References

Babuška, V. & Cara, M., 1991. *Seismic Anisotropy in the Earth*, Kluwer Academic Publisher, London.

Backus, G.E., 1962. Long-wave anisotropy produced by horizontal layering, *J. Geophys. Res.*, **66**, 4427-4440.

Baptie, B., Crampin, S. & Liu, E., 1995. Displaying shear-wave splitting in cross-hole surveys for materials with combinations of EDA and PTL anisotropies, *Can. J. Explor. Geophys.*, **29**, 227-235.

Bulant, P. & Klimeš, L., 2004. Comparison of quasi-isotropic approximations of the coupling ray theory with the exact solution in the 1-D anisotropic 'oblique twisted crystal' model, *Stud. Geophys. Geod.*, **48**, 97-116.

Coates, R.T. & Chapman, C.H., 1990. Quasi-shear wave coupling in weakly anisotropic 3-D media. *Geophys. J. Int.*, **103**, 301-320.

Farra, V. 2004. Improved first-order approximation of group velocities in weakly anisotropic media, *Stud. Geophys. Geod.*, **48**, 199-213.

Farra, V., 2005. First-order ray tracing for qS waves in inhomogeneous weakly anisotropic media, *Geophys. J. Int.*, **161**, 309-324, doi: 10.1111/j.1365-246X.2005.02570.x.

Godfrey, N.J., Christensen, N.I. & Okaya, D.A., 2000. Anisotropy of schists: Contribution of crustal anisotropy to active source seismic experiments and shear wave splitting observations, *J. Geophys. Res.*, **105**, No. B12, 27.991-28.007.

Helbig, K., 1994. *Foundations of Anisotropy for Exploration Seismics*, Pergamon, N.Y.

Hudson, J.A., 1981. Wave speeds and attenuation of elastic waves in material containing cracks, *Geophys. J. R. astr. Soc.*, **64**, 133-150.

Jost, M.L. & Hermann, R.B., 1989. A student's guide to and review of moment tensors, *Seismol. Res. Lett.*, **60**, 37-57.

Julian, B.R., Miller, A.D. & Foulger, G.R., 1998. Non-double-couple earthquakes, 1. Theory, *Rev. Geophys.*, **36**, 525-549.

Kawasaki, I. & Tanimoto, T., 1981. Radiation patterns of body waves due to the seismic dislocation occurring in an anisotropic source medium, *Bull. Seismol. Soc. Am.*, **71**, 37-50.

Klimeš, L. & Bulant, P., 2004. Errors due to the common ray approximations of the coupling ray theory, *Stud. Geophys. Geod.*, **48**, 117-142.

Korn, G.A. & Korn, T.M., 2000. *Mathematical Handbook for Scientists and Engineers*, Dover Publications, N.Y.

Kravtsov, Yu.A. & Orlov, Yu.I., 1990. *Geometrical Optics of Inhomogeneous Media*, Springer-Verlag, New York.

Maxwell, S.C. & Urbancic, T.I., 2001. The role of passive microseismic monitoring in the instrumented oil field, *Leading Edge*, **20**, 636-640.

Musgrave, M.J.P., 1970. *Crystal Acoustics*, Holden-Day, London.

Pšenčík, I. & Dellinger, J.A., 2001. Quasi-shear waves in inhomogeneous weakly anisotropic media by the quasi-isotropic approach: A model study, *Geophysics*, **66**, 308-319.

Pšenčík, I. & Gajewski, D., 1998. Polarization, phase velocity, and NMO velocity of qP-waves in arbitrary weakly anisotropic media, *Geophysics*, **63**, 1754-1766.

Rabbel, W., Beilecke, T., Bohlen, T., Fischer, D., Frank, A., Hasenclever, J., Borm, G., Kück, J., Bram. K., Druivenga, G., Lüschen, E., Gebrande, H., Pujol, J. & Smithson, S., 2004. Superdeep vertical seismic profiling at the KTB deep drill hole (Germany): Seismic close-up view of a major thrust zone down to 8.5 km depth, *J. Geophys. Res.*, **109**, B09309, doi: 10.1029/2004JB002975.

Rössler, D., Rümpker, G. & Krüger, F., 2004. Ambiguous moment tensors and radiation patterns in anisotropic media with applications to the modeling of earthquake mechanisms in W-Bohemia, *Stud. Geophys. Geod.*, **48**, 233-250.

Rutledge, J.T. & Phillips, W.S., 2003. Hydraulic stimulation of natural fractures as revealed by induced microearthquakes, Carthage Cotton Valley gas field, east Texas, *Geophysics*, **68**, 441-452.

Shearer, P.M. & Chapman, C.H., 1989. Ray tracing in azimuthally anisotropic media – I. Results for models of aligned cracks in the upper crust, *Geophys. J. Int.*, **96**, 51-64.

Šílený, J. & Vavryčuk, V., 2002. Can unbiased source be retrieved from anisotropic waveforms by using an isotropic model of the medium?, *Tectonophysics*, **356**, 125-138.

Thomsen, L., 1986. Weak elastic anisotropy, *Geophysics*, **51**, 1954-1966.

Tsvankin, I., 2001. *Seismic Signatures and Analysis of Reflection Data in Anisotropic Media*, Pergamon, N.Y.

Tsvankin, I., & Thomsen, L., 1994. Nonhyperbolic reflection moveout in anisotropic media, *Geophysics*, **59**, 1290-1304.

Vavryčuk, V., 2001. Inversion for parameters of tensile earthquakes, *J. Geophys. Res.*, **106**, No. B8, 16.339-16.355.

Vavryčuk, V., 2002. Non-double-couple earthquakes of January 1997 in West Bohemia, Czech Republic: Evidence of tensile faulting, *Geophys. J. Int.*, **149**, 364-373.

Vavryčuk, V., 2004. Inversion for anisotropy from non-double-couple components of moment tensors, *J. Geophys. Res.*, **109**, B07306, doi:10.1029/2003JB002926.

Vavryčuk, V., 2005. Focal mechanisms in anisotropic media, *Geophys. J. Int.*, **161**, 334-346, doi: 10.1111/j.1365-246X.2005.02585.x.

Vavryčuk, V. & Pšenčík, I., 1998. *PP* wave reflection coefficients in weakly anisotropic elastic media, *Geophysics,* **63**, No. 6, 2129-2141.